

H α KINEMATICS OF THE ISOLATED INTERACTING GALAXY PAIR *KPG* 486 (*NGC* 6090).

M. M. Sardaneta,¹ M. Rosado,² and M. Sánchez-Cruces¹

Draft version: August 9, 2021

RESUMEN

En imágenes del óptico, el par de galaxias aislado no estudiado ampliamente, *KPG* 486 (*NGC* 6090), muestra características similares al par de galaxias Las Antenas (*NGC* 4038/39). Para comparar la distribución del gas ionizado, morfología y comportamiento cinemático y dinámico entre ambos pares de galaxias, se presentan observaciones en la línea de emisión H α de *NGC* 6090 adquiridas con el interferómetro Fabry-Perot de barrido, PUMA. Para cada galaxia en *NGC* 6090 se obtuvieron varios parámetros cinemáticos, su campo de velocidades y su curva de rotación, además se analizaron algunas de las perturbaciones inducidas por su encuentro. Se verificó la consistencia de estos resultados comparándolos con los de la literatura. La comparación de los resultados de *NGC* 6090 con los de un análisis cinemático similar previo a Las Antenas destacó grandes diferencias entre estos pares de galaxias.

ABSTRACT

In optical images, the not amply studied isolated interacting galaxy pair *KPG* 486 (*NGC* 6090) displays similar features to the galaxy pair The Antennae (*NGC* 4038/39). To compare the distribution of ionized hydrogen gas, morphology and kinematic and dynamic behaviour between both galaxy pairs, we present observations in the H α emission line of *NGC* 6090 acquired with the scanning Fabry-Perot interferometer, PUMA. For each galaxy in *NGC* 6090 we obtained several kinematic parameters, its velocity field and its rotation curve, we also analysed some of the perturbations induced by their encounter. We verified the consistency of our results by comparing them with kinematic results from the literature. The comparison of our results on *NGC* 6090 with those obtained in a previous similar kinematic analysis made for The Antennae highlighted great differences between these galaxy pairs.

Key Words: galaxies: individual (*NGC* 6090) — galaxies: interactions — galaxies: kinematics and dynamics — methods: data analysis — techniques: interferometric

1. INTRODUCTION

Instead of evolving in isolation, galaxies are found in clusters and groups and they can interact quite strongly with their nearby companions. These interactions can have a profound impact on the properties of galaxies, resulting

¹Aix Marseille Univ, CNRS, CNES, LAM, Marseille, France.

²Instituto de Astronomía, UNAM, México.

in intense bursts of star formation, the onset of quasar-like activity in galactic nuclei and perhaps even the complete transformation of spiral galaxies into elliptical galaxies. Studies of galaxies in the early universe show a significant fraction of interacting and merging systems, and theories of cosmological structure formation indicate that most galaxies have had some form of strong interaction during their lifetime. Rather than being rare events, galaxy interactions may be the dominant process shaping the evolution of the galaxy population in general (Mihos 2000).

The evolution and interaction of galaxies is governed by gravitational effects. Morphologically, in the interacting galaxies there are large bridges and tails, stellar bars and/or increased spiral structures and, commonly, the bodies of galaxies are distorted (Schweizer 1986). Toomre & Toomre (1972), through numerical simulations, it was established that the gravitational interaction with another galaxy may be the source of not only spiral structures, but also of the filamentary structure, which they called ‘tidal tails’, thus, gravity is solely responsible for these large and thin tails and several other deformations seen in several surveys (e.g. Arp 1966; Karachentsev 1987; Vorontsov-Velyaminov et al. 2001).

Numerical simulations show that during a merger, tidal forces from a companion galaxy trigger the formation of a bar in the disc of a perturbed galaxy (Noguchi 1987; Salo & Laurikainen 2000a,b; Renaud et al. 2015). The bar acts to trigger starburst activity by rapidly funnelling large amounts of gas to the nuclear region (Barnes & Hernquist 1992; Dinshaw et al. 1999; Gabbasov et al. 2014; Martin & Soto 2016). When a bar is clearly observable in the stellar component, the gas dynamics shows very distinctive characteristics, corresponding to elliptical and non-circular orbits, the isoveLOCITIES contour curves are deformed symmetrically, then the inclination of the central isoveLOCITY contour curve along the minor axis is one of the main features used to identify a bar (Bosma 1981; Combes et al. 2002).

The simplest case in the process of galaxy interactions are the isolated galaxy pairs, which are systems composed of two galaxies located closely in the space that the gravitational effect of their nearest neighbours can be neglected relative to the gravitational effects exerted between each other (Fuentes-Carrera et al. 2004; Rosado et al. 2011; Gabbasov et al. 2014). Systematic research on double galaxies provide us with important information about the conditions of formation and properties of the evolution of galaxies (Karachentsev 1987).

Obtaining kinematic information from interacting galaxies is useful for understanding the effect that the interaction can have on each of the members of the pair (Fuentes-Carrera et al. 2004, 2007; Repetto et al. 2010). In highly disturbed velocity fields, double nuclei, double kinematic gas components and high amplitude discrepancies between both sides of the rotation curves imply strong galaxy-galaxy interactions or mergers. On the other hand, stellar and gaseous major axes misalignments and tidal tails suggest collisions that may not always lead to merging (Amram et al. 2003; Torres-Flores et al. 2014).

From the observational point of view, most of the kinematic works on interacting galaxies have been carried out using long-slit spectroscopy along certain positions (e.g. Günthardt et al. 2016), restricting kinematic information from only few points on the galaxy. However, for an asymmetric perturbed system, it is important to obtain the kinematic information from large portions of the disc using observational techniques such as integral field spectroscopy with a scanning Fabry-Perot interferometer (FP). In this way, the extended kinematic information can help us determine the interaction process which has been produced on each of the members of the interacting system, in addition to the fact that, sometimes the axial symmetry of each galaxy is lost during the interaction (Fuentes-Carrera et al. 2004, 2015; Epinat et al. 2008).

NGC 6090

The isolated interacting galaxy pair *KPG* 486 (*NGC* 6090) has been described as a double nuclei system with an asymmetric disc and two long tidal tails of ~ 60 kpc in length (e.g. Dinshaw et al. 1999). At optical wavelengths, this galaxy system looks like the *NGC* 4038/39 galaxy system (The Antennae) (e.g. Toomre & Toomre 1972; Hummel et al. 1987; Martin et al. 1991; Mazzarella & Boroson 1993; Dinshaw et al. 1999; Bryant & Scoville 1999). This feature can be observed in the upper panel of Figure 1 which shows the optical image of *NGC* 6090 taken from the Digitized Sky Survey (DSS) in a field of view of 4 arcmin.

In radio-wavelengths *NGC* 6090 is described as a pair of interacting spirals separated by 0.14 arcsec with nuclei in contact and enormous curved wings (Martin et al. 1991). Meanwhile, molecular gas appears elongated and aligned along the direction of the nuclei as a rotating disc (Wang et al. 2004) or ring (Bryant & Scoville 1999; Sugai et al. 2000). The position angle of that disc is $\sim 60^\circ$ with a major axis length of ~ 3.4 arcsec, the CO source appears to peak between the radio nuclei rather than on one of them (Bryant & Scoville 1999) and the molecular gas component does not appear to belong to any of the galaxies in the system based on the kinematics (Wang et al. 2004).

Due to the interaction evidence that *NGC* 6090 shows it was defined as a merger by Chisholm et al. (2015). But also, *NGC* 6090 has been defined as a galaxy system in an intermediate stage of merging or pre-merging too because, in addition of its two nuclei and tidal tails, the galaxy system has an identifiable bridge (Miralles-Caballero et al. 2011). In the near-infrared, the galaxies that make up *NGC* 6090 are seen as follows: *NGC* 6090 *NE* has a distorted spiral structure and evidence of a stellar bar and *NGC* 6090 *SW* looks like an irregular galaxy and the position of its nucleus is still under discussion (Dinshaw et al. 1999; Cortijo-Ferrero et al. 2017). In Table 1 we listed the general parameters of *NGC* 6090 which have been reported only for a single galactic system hitherto.

To investigate the distribution of ionized hydrogen gas, morphology, and kinematic and dynamic behaviour of the galaxy system *NGC* 6090, we obtained a FP data cube spectrally centered on the H α emission line of the

system. In this paper we present the analysis of the $H\alpha$ image, the velocity field and dispersion velocity map of the pair of galaxies *NGC* 6090, as well as the rotation curves obtained for each member. Lastly, we comment on our results and those found in the literature and compare the kinematic characteristics of the galaxy system *NGC* 6090 with those of The Antennae made by Amram et al. (1992).

This paper is organized as follows: in § 2 there is an overview of the observational parameters and the reduction process; in § 3, we present the morphological features of *NGC* 6090 observed from its $H\alpha$ monochromatic and continuum maps; § 4 is devoted to the kinematic analysis made from our FP data, there are shown the derived velocity fields, the associated rotation curve of each member of the galaxy system *NGC* 6090 and we analyse the non-circular motions of each galaxy throughout the velocity dispersion map of the system; § 5 is dedicated to the dynamical analysis including the computation of the mass of each galaxy. A discussion is presented in § 6, and our conclusions are given in § 7.

In this paper, we considered $H_0 = 75 \text{ km s}^{-1} \text{ Mpc}^{-1}$ (Condon et al. 1990) and adopted a distance of 118 Mpc for *NGC* 6090.

TABLE 1
PARAMETERS OF THE GALAXY SYSTEM *NGC* 6090.

Parameters	<i>NGC</i> 6090 system
Coordinates (J2000)	$\alpha = 16^h 11^m 40.7^s$ $\delta = +52^\circ 27' 24''^a$
Other names	<i>KPG</i> 486 ^{a,c} <i>NGC</i> 6090 ^a UGC 10267 ^a Mrk 496 ^a
Morphological type	G Pair ^a Multiple galaxy ^b Merger, double nucleus ^e Merger ^g
Mean heliocentric	8906 ^a
radial velocity (km s ⁻¹)	8855 ^b
Distance (Mpc)	122 ^{d(*)} 123.3 ^{e(*)} 128 ^{g(**)} 127.7 ^{h(**)}
L _{IR} (L _⊙)	3×10 ¹¹ ^f
m _b	14.36 ^a
D _{25/2} (arcmin)	4.36 ^b
Photometric nuclear separation (arcsec)	5.4 ^c

^aNASA/IPAC (2014)¹; ^bHyperLeda²; Makarov et al. (2014); ^cKarachentsev (1987); ^dCondon et al. (1990); ^eBryant & Scoville (1999); ^fAcosta-Pulido et al. (1996); ^gChisholm et al. (2015); ^hCortijo-Ferrero et al. (2017).

(*) Distance $D = v/H_0$ computed using $H_0 = 75 \text{ km s}^{-1} \text{ Mpc}^{-1}$.

(**) Distance obtained from $z = 0.02930$ with $H_0 = 70 \text{ km s}^{-1} \text{ Mpc}^{-1}$.

¹*NASA/IPAC Extragalactic Data Base* (NED) is operated by the Jet Propulsion Laboratory, California Institute of Technology, under contract with the National Aeronautics and Space Administration. <https://ned.ipac.caltech.edu/>

²HyperLeda: <http://leda.univ-lyon1.fr/>

2. OBSERVATIONS AND DATA REDUCTIONS

Our observations to *NGC* 6090 were performed in July 2015 with the $f/7.5$ Cassegrain focus at the 2.1 m telescope at the Observatorio Astronómico Nacional in San Pedro Mártir, Baja California, México (OAN-SPM for its acronym in Spanish) using the scanning Fabry-Perot interferometer, PUMA (Rosado et al. 1995). PUMA is a focal reducer built at the Instituto de Astronomía-UNAM used to make images and Fabry-Perot interferometry of extended emission cosmical sources. The FP used is an ET-50 (Queensgate Instruments) with a servostabilization system having a free spectral range of 19.9 \AA (909 km s^{-1}) at $\text{H}\alpha$. The effective finesse of PUMA is ~ 24 which implies a sampling spectral resolution in $\text{H}\alpha$ of 0.414 \AA (19.0 km s^{-1}) achieved by scanning the interferometer free spectral range through 48 different equally spaced channels (Rosado et al. 1995). However, due to the parallelism of the FP mirrors during the data acquisition for the observations particularly to *NGC* 6090, the measured finesse for this data cube was ~ 10 which leads a sampling spectral resolution of 0.97 \AA (44.1 km s^{-1}) at $\text{H}\alpha$.

We used a 2048×2048 CCD detector with a pixel scale of 0.317 arcsec and we set a 4×4 binning to enhance the signal, obtaining a 512×512 pixel window inside of a field of view of 10 arcmin . So, we obtained a final spatial sampling per pixel of 1.27 arcsec which is slightly better than the average seeing of 1.67 arcsec . To isolate the redshifted $\text{H}\alpha$ emission line, it was utilised an interference filter centred at 6819 \AA with FWHM of 86 \AA . Thus, we obtained an $\text{H}\alpha$ data cube with a total exposure time of 72 minutes (90 s per channel).

Then, in order to avoid phase wavelength dependence of the FP layers is necessary to calibrate the data cube in wavelength. So, we used a Ne lamp whose line at 6717 \AA is close to the redshifted nebular wavelength to obtain a calibration cube at the end of the observation. The parabolic phase map was computed from the calibration cube in order to obtain the reference wavelength for the line profile observed inside each pixel. The instrumental and observational parameters are listed in Table 2.

For the data reduction and analysis we used the ADHOCw³ software to make the standard corrections on the cube: removal of cosmic rays and bias subtraction, subtraction of the OH sky lines at 6828.5 \AA , 6842.2 \AA and 6863.9 \AA (Chamberlain 1961; Krassovsky et al. 1962) and the application of a spectral Gaussian smoothing with $\sigma = 57 \text{ km s}^{-1}$ on the data cube. We applied IRAF⁴ tasks as IMEXAMINE to determine the average seeing of our data and MSCSETWCS to add the World Coordinate System (WCS) to the resulting maps of *NGC* 6090. To complete the data analysis we used our own Python scripts.

The FP scanning process allows us to obtain a flux value in arbitrary units at pixel level for each of the 48 scanning steps. The calibration in wavelength was fixed for each profile at each pixel using the calibration data cube. Thus,

³<http://cesam.lam.fr/fabryperot/index/software> developed by J. Boulesteix.

⁴IRAF: ‘Image Reduction and Analysis Facility’

<http://iraf.noao.edu/>

the intensity profile found throughout the scanning process contains information about the monochromatic emission (ionized gas emitting at H α), the continuum emission of the object, as well as the velocity of the ionized gas. The computation of the image of the continuum was made considering the average of the 3 lowest intensities of the 48 channels of the cube (e.g. Vollmer et al. 2000; Fuentes-Carrera et al. 2004; Repetto et al. 2010; Rosado et al. 2013; Cárdenas-Martínez & Fuentes-Carrera 2018). For the monochromatic image, the intensity of the H α line was obtained by integrating the maximum value of the line profile for each pixel.

ADHOCw calculates the radial velocity fields using the barycentre of the profile of the H α line for each pixel with an accuracy in central velocities of $\pm 5 \text{ km s}^{-1}$. We masked the velocity field including only a rectangular area that contains the part of the radial velocity map corresponding to *NGC* 6090. Then, we superimposed the radial velocity profiles on the resulting velocity field and masked the radial velocity field based on the signal-to-noise ratio of each pixel, whose values are in the range from 24 in the centre of the galaxy system until 4 in the very external pixels.

In addition to the data cube, we obtained a direct H α image of *NGC* 6090 having the FP outside the optical path and with the same filter with exposure time of 90 seconds.

TABLE 2

INSTRUMENTAL AND OBSERVATIONAL PARAMETERS

Parameter	Value
Telescope	2.1 m (OAN, SPM)
Instrument	PUMA
Detector	Site3 CCD
Detector size	2048×2048 pix
Image scale (binning 4×4)	1.27 arcsec/pix
Scanning FP interferometer	ET-50
Finesse	~ 10
FP interference order at H α	330
Free spectral range at H α	19.9 Å (909 km s $^{-1}$)
Spectral sampling resolution at H α	0.97 Å (44.1 km s $^{-1}$)
Interference filter	6819 Å (FWHM = 86 Å)
Total exposure time	72 min
Calibration line	6717 Å (Ne)
Average seeing	1.67 arcsec

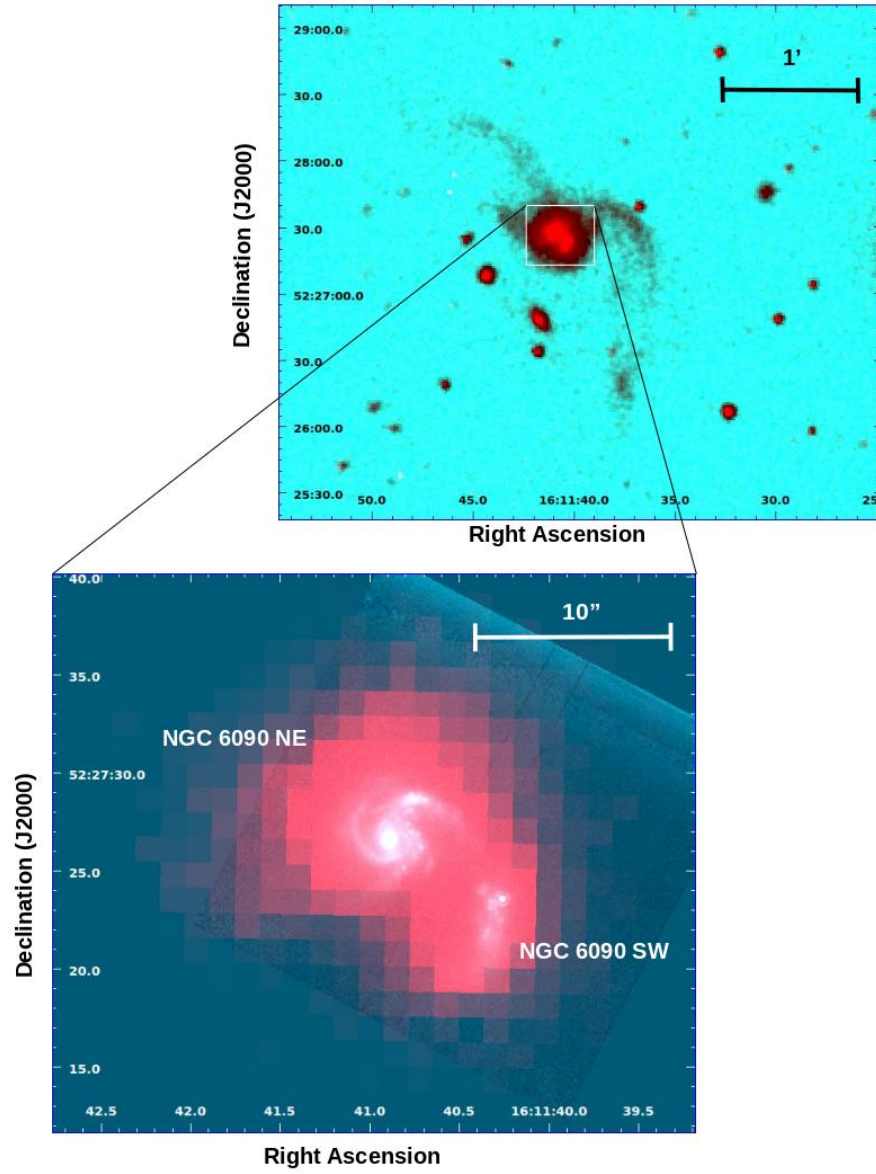


Fig. 1. Above: Image from the Digitized Sky Survey (DSS) in a 4 arcmin field of view centred in the galaxy system *NGC* 6090 over which was superimposed in red the $H\alpha$ direct image taken with a 6819 \AA filter with FWHM of 86 \AA obtained from the PUMA in its direct image mode at the 2.1 m telescope from the Observatorio Astronómico Nacional in San Pedro Mártir (OAN-SPM), Baja California, México. Below: $2.22 \mu\text{m}$ image from the Near-Infrared Camera Multi-Object on the *Hubble Space Telescope* (NICMOS/HST) over which was superimposed in red the $H\alpha$ direct image from OAN-SPM in a 28 arcsec field of view centred on *NGC* 6090.

3. MONOCHROMATIC AND CONTINUUM IMAGES

On the DSS optical image of *NGC* 6090 (upper panel of Figure 1) we superimposed the direct H α image obtained with PUMA. The ionized gas emitting at H α that we detected was found within the central area of the object, which has 20.32 arcsec per side, i.e. 16 pixels per side, where 1 pix = 1.27 arcsec = 0.726 kpc. The mean heliocentric radial velocity that we determined in this work to the galactic system *NGC* 6090 is 8885 km s⁻¹. We did not detect ionized gas emitting at H α in the tidal tails (antennae), so we limited our kinematic analysis to the central area of *NGC* 6090 without taking into account the antennae. In the bottom panel of Figure 1 we show the *NICMOS/HST* 2.22 μ m image whose 22 arcsec field of view matches with our results.

To have a sight about the morphology of *NGC* 6090 that the PUMA data show, the contours of the H α continuum (Figure 2 left panel) and monochromatic (Figure 2 right panel) emissions of *NGC* 6090 were superimposed on the *NICMOS/HST* image.

The coordinates of the continuum maximum of *NGC* 6090 *NE* are $\alpha_{J2000} = 16^h 11^m 40.8^s$, $\delta_{J2000} = +52^\circ 27' 27''.32$, and the maximum H α monochromatic emission is in $\alpha_{J2000} = 16^h 11^m 40.8^s$, $\delta_{J2000} = +52^\circ 27' 27''.0$. For *NGC* 6090 *NE*, we can observe that the ionized gas emitting at H α has greater presence towards the west, i.e. towards its companion galaxy, while, the isophotes of the continuum show that the stellar population has greater presence towards the east. In addition, in *NGC* 6090 *NE* we can observe that the isophotes of the continuum are symmetrical with respect to the photometric position angle (PA), which is the angle of the major axis of the continuum with respect to the north in counter-clockwise and whose value is $\simeq 0^\circ$ in this case. The pattern of the isophotes suggest the likely presence of a stellar bar.

For the galaxy *NGC* 6090 *SW*, the coordinates of the photometric maximum are $\alpha_{J2000} = 16^h 11^m 40.4^s$, $\delta_{J2000} = +52^\circ 27' 22''.21$ and the coordinates of the H α monochromatic maximum are $\alpha_{J2000} = 16^h 11^m 43.3^s$, $\delta_{J2000} = +52^\circ 27' 23''.0$. For this galaxy, we can observe that the continuum has greater presence towards the south, the opposite side of its companion, and also it is accumulated towards the opposite direction of its H α maximum emission. Moreover, we can note that the H α monochromatic maximum is nearer of the the knot described in the literature as the maximum of the 2.22 μ m image (e.g. Dinshaw et al. 1999) than the photometric center of the galaxy, what has created controversy in the literature about the position of the nuclei of *NGC* 6090 *SW*.

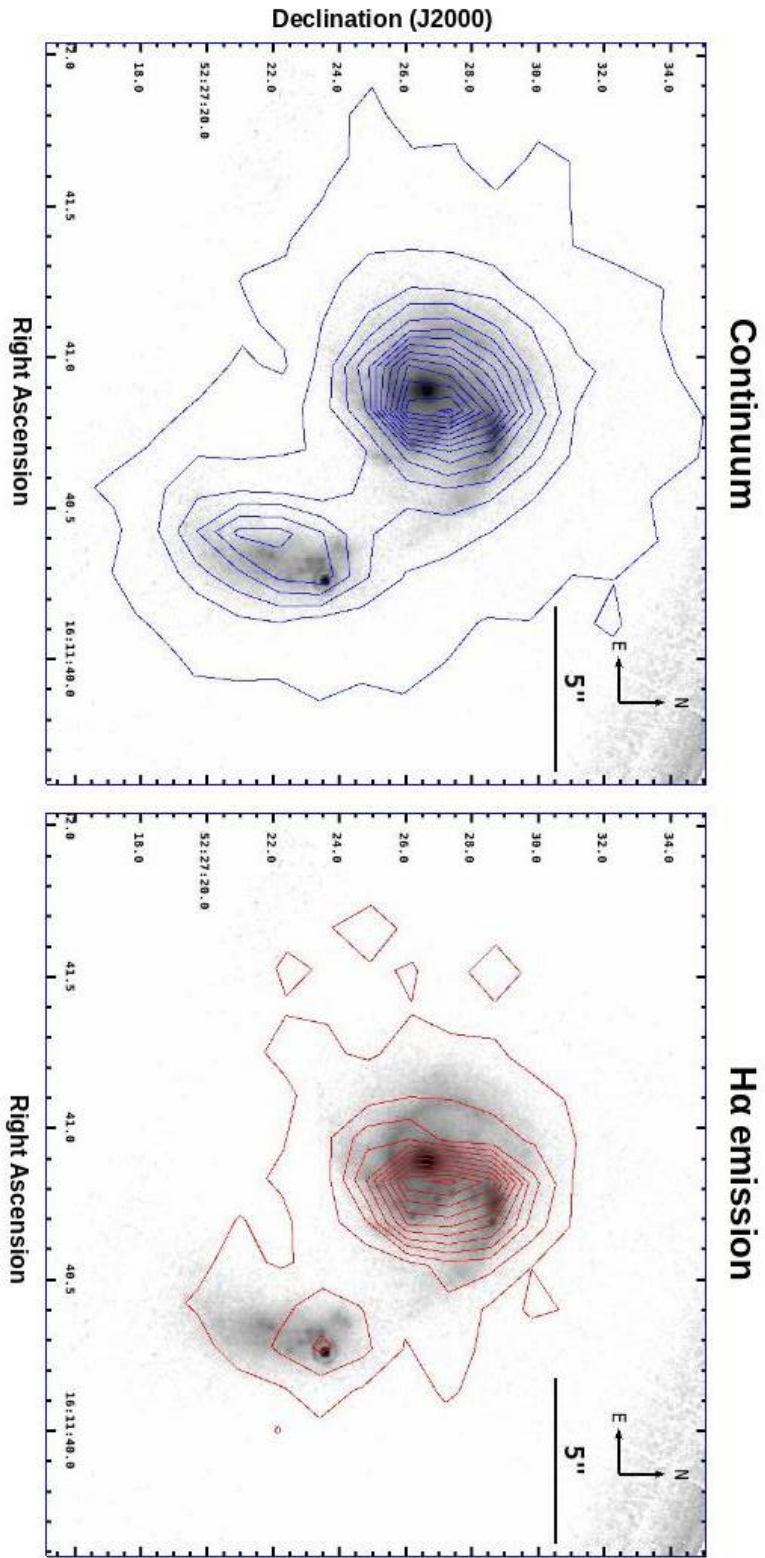


Fig. 2: Left: contours of the continuum linearly spaced from 1500 to 10000 ADU obtained from the H α data cube from the scanning FP interferometer, PUMA overlaid on the NICMOS/HST 2.22 μ m image in a 22 arcsec field of view centred on NGC 6090. Right: contours of the H α monochromatic image linearly spaced from 4000 to 240000 ADU obtained with PUMA overlaid on the NICMOS/HST 2.22 μ m image in a 22 arcsec field of view centred on NGC 6090.

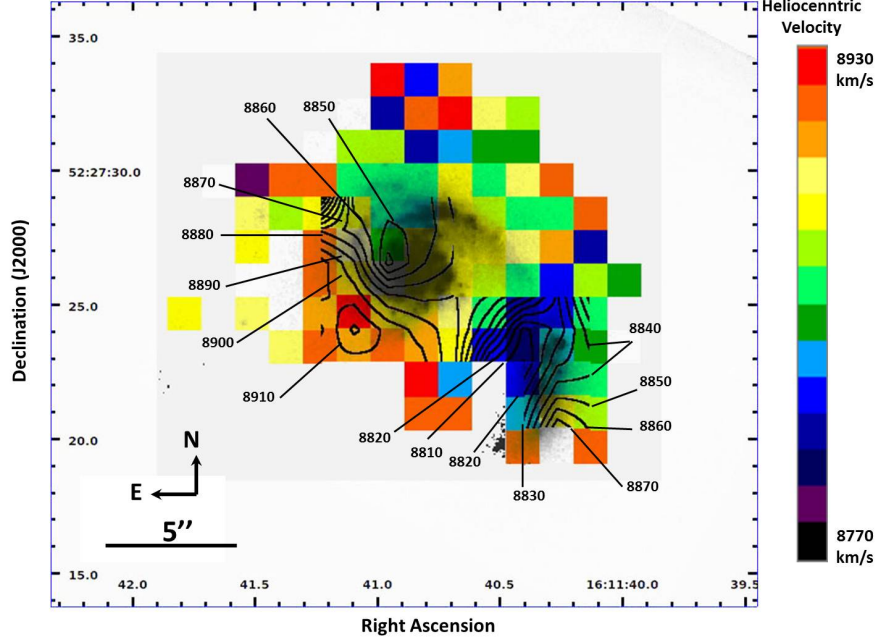


Fig. 3. Velocity field acquired with the H α data cube observation obtained with the scanning FP interferometer, PUMA, in a 26 arcsec field of view centred in *NGC* 6090. On the velocity field are overlaid, firstly, the NICMOS/HST 2.22 μm image and, secondly, the isovelocity contours of each galaxy which are linearly spaced by a factor of 10 starting from 8810 km s^{-1} . Each isovelocity is labelled in km s^{-1} units.

4. KINEMATIC RESULTS

4.1. Velocity fields

In the previous section was shown that the ionized gas emitting at H α does not have the same morphology than the continuum emission, as a consequence of this phenomenon due to the interaction between the galaxies, we do not expect that all the photometric and kinematic parameters exactly match. In Figure 3, which shows the velocity field of *NGC* 6090 where its isovelocity contour curves and the 2.22 μm image were superimposed, is possible to notice the velocity field of two independent galaxies, i.e. the velocity field of *NGC* 6090 presents two velocity fields ordered roughly on each one of its photometric maxima. Also, each velocity field has distortions towards the outside, mainly toward the northern side of both galaxies.

For *NGC* 6090 NE, the values of the radial velocities within its ordered velocity field, which reaches a radius of $R = 5.6$ arcsec, are in the range from 8783 to 8919 km s^{-1} . For *NGC* 6090 SW, the radial velocities are in the range from 8799 to 9143 km s^{-1} within its velocity field which is ordered up to a radius of $R = 4.5$ arcsec. Furthermore, for *NGC* 6090 NE, in Figure 3 we observe that the isovelocity contour curves of the disc of the galaxy are not

symmetric with respect to the kinematic minor axis, this feature added to the morphology signed by the continuum contours described in previous section suggests the presence of a stellar bar in agreement with the criteria proposed by Bosma (1981).

4.2. Rotation curves

From the morphological and kinematic features described in previous sections, we can argue that we have detected two independent galaxies inside the *NGC* 6090 galactic system. In this kind of interacting systems is seen that the radial motions such as inflows/outflows or motions perpendicular to the galactic disc are second order effects, otherwise the discs would be destroyed. We started studying the circular motion of each galaxy in *NGC* 6090, which corresponds to the most basic motion that can be assumed in a disc galaxy. In this way, the rotation curve of each galaxy was obtained from the kinematic data acquired with our FP observations with the ADHOCw software, which computes the radial velocity of the galaxies in every single pixel using the barycentre of the $H\alpha$ profile observed in each pixel.

In doing so, we use the geometric and kinematic assumptions proposed by Mihalas & Binney (1981). Supposing that each galaxy has a well-defined disc and the system rotates about an axis that is perpendicular to the galactic plane which is inclined an angle i to the plane of the sky, with the polar coordinate systems (R, θ) in the plane of the galaxy and (ρ, ϕ) in the plane of the sky, locating the origin at the point where the rotation axis embeds the plane of the sky, the radial velocity (V_{obs}) measured at (ρ, ϕ) is $V_{obs}(\rho, \phi) = V_{sys} + V_r(R, \theta) \sin \theta \sin i + V_\Theta(R, \theta) \cos \theta \sin i + V_z(R, \theta) \cos i$, where $R^2 = \rho^2(\cos^2 \phi + \sec^2 i \sin^2 \phi)$ and $\tan \phi = \sec i \tan \theta$, with V_{sys} the mean heliocentric radial velocity of the system as a whole (that is, of its centre of mass); V_r and V_Θ are the radial and tangential velocities in the plane, respectively, and V_z is the velocity perpendicular to the plane. Given that rotation is generally the dominant form of motion in disc galaxies, we assumed V_r and V_z equal to zero. Moreover, under the assumption that there is axial symmetry about the centre of galaxy, V_Θ will depend only on R . Thus, the tangential velocity in the plane of the galaxy (V_Θ) is obtained with the radial velocity V_{obs_k} of the k th region on the galaxy in terms of observable quantities:

$$V_\Theta(R_k) = \frac{V_{obs_k} - V_{sys}}{\cos \theta_k \sin i}, \quad (1)$$

where R_k and θ_k are given in terms of the coordinates ρ_k and ϕ_k of the k th galaxy region on the sky which corresponds to the k th pixel of the velocity field that was obtained with our FP observations.

The ADHOCw software averages the measured velocity of the pixels that are at the same distance from the kinematic center along the major axis indicating the dispersion associated to this average with bars on the points of the rotational observed curves. In order to avoid strong dispersions associated to the points of the rotation curves there were considered the pixels within

TABLE 3
ROTATION CURVE PARAMETERS AND THE MASS RANGE OF
EACH GALAXY IN *NGC* 6090 PAIR.

Parameters	<i>NGC</i> 6090 <i>NE</i>	<i>NGC</i> 6090 <i>SW</i>
Coordinates (J2000)	$\alpha = 16^h 11^m 40.84^s$ $\delta = +52^\circ 27' 26''.94$	$\alpha = 16^h 11^m 40.42^s$ $\delta = +52^\circ 27' 22''.21$
Distance (Mpc)	118	118
Systemic velocity (km s $^{-1}$)	8880	8890
Max. Rotation Velocity (km s $^{-1}$)	130 \pm 5	132 \pm 5
Kinematic <i>PA</i> ($^\circ$)	150 \pm 3	26 \pm 3
Inclination ($^\circ$)	13.9 \pm 0.5	64.8 \pm 0.5
Radius (arcsec)	5.6	4.5
Radius (kpc)	3.2	2.6
Mass (M_\odot)	0.76 $\times 10^{10}$ to 1.26 $\times 10^{10}$	0.63 $\times 10^{10}$ to 1.05 $\times 10^{10}$

an angular sector along the kinematic major axis (e.g. Fuentes-Carrera et al. 2004, 2007; Repetto et al. 2010) as is shown in left panels of Figure 4. Then, by assuming that each galaxy has a well-defined disc, due to its inclination it would look like an ellipse on the plane sky with apparent axis lengths a and b , so its inclination can be computed by $i = \cos^{-1}(b/a)$. We applied the ELLIPSE task of IRAF to the 2.22 μm image to estimate the inclination of the galaxies from the isophotal ellipses traced on these images. Finally, we considered that the systemic velocity of each galaxy is in agreement to the radial velocity of its own kinematic centre.

Table 3 contains the parameters that we used to calculate the rotation curve of each galaxy, the listed values correspond to those values with which we obtained the rotation curves from our observations, changes in these values would result in scattered points in the rotation curves instead of symmetric rotation curves.

The rotation curve of *NGC* 6090 *NE* presented in the upper right panel of Figure 4 was obtained with pixels in the velocity field within an angular sector of 30° around the kinematic major axis of the galaxy as is marked in the upper left panel of Figure 4. The physical coordinates of the kinematic centre, derived as the position around the photometric centre at which the scatter in rotation curve is minimized, are $\alpha_{\text{J2000}} = 16^h 11^m 40.84^s$, $\delta_{\text{J2000}} = +52^\circ 27' 26''.94$. The kinematic centre used to compute the rotation curve in this galaxy matches the photometric centre within 0.4 arcsec. Using ADHOCw software, the kinematic parameters that give us the most symmetric, smooth and low scattered curve inside of the radius $R = 5.6$ arcsec are $PA = 150^\circ \pm 3$, $i = 13.9^\circ \pm 0.5$, and $V_{\text{sys}} = 8880 \text{ km s}^{-1}$. We determined that the heliocentric distance to this galaxy is 118 Mpc through the Hubble law (Hubble 1936). The rotation curve shows that the north of the galaxy is blue-shifted, i.e. in the

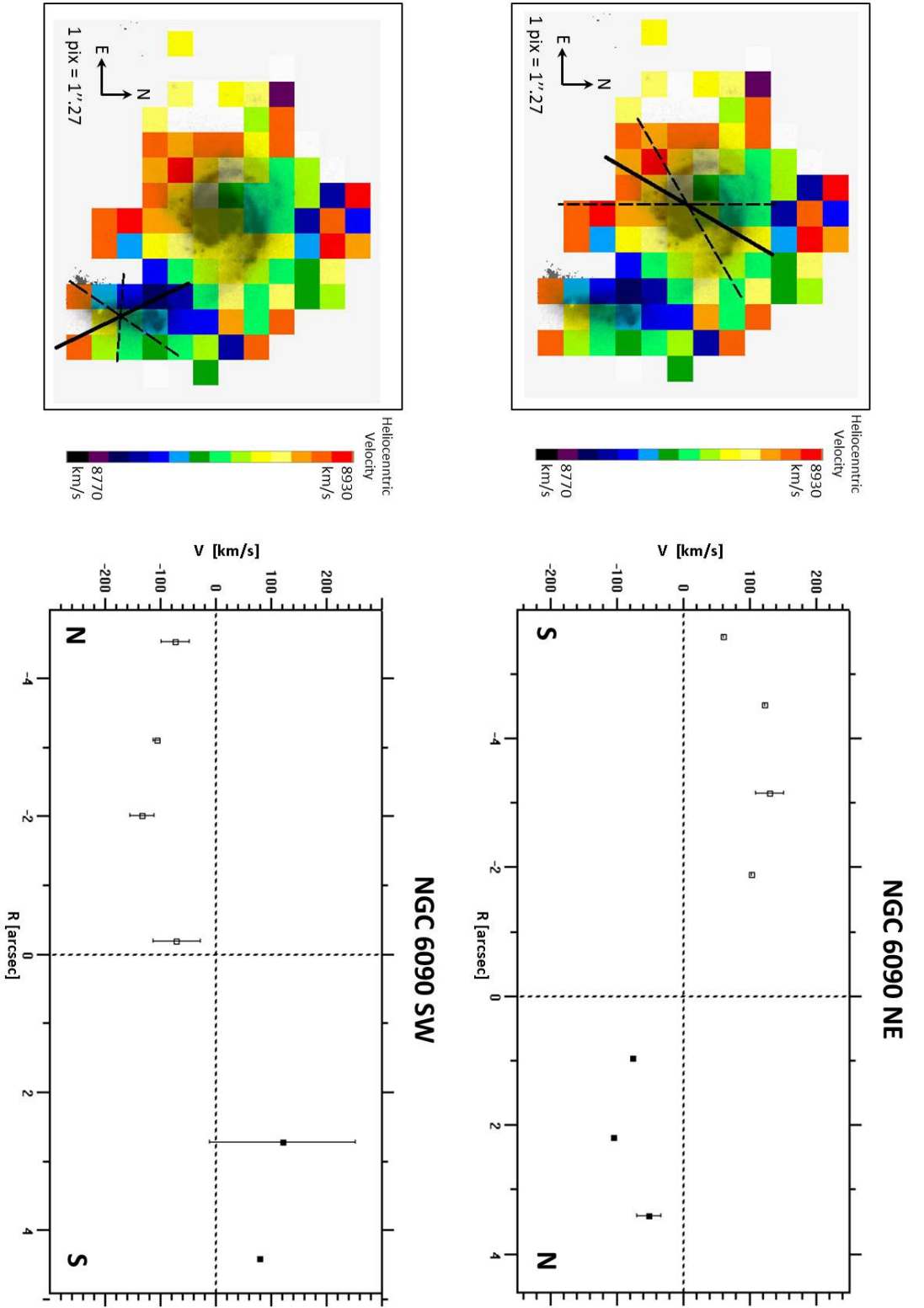


Fig. 4: Left panels show the velocity maps acquired with the H α data cube obtained with the scanning FP interferometer, PUMA, in a 22 arcsec field of view, on these maps was superimposed the NICMOS/HST 2.22 μ m image as a frame of reference for the position of galaxy components in the galactic pair; then, on each map, the solid line represents the major kinematic axis which indicates the kinematic PA and the dashed lines represent the sector angle that was considered for the computation of the rotation curve of each galaxy: *NGC 6090 NE* above and *NGC 6090 SW* below. In right panels are shown the rotation curves of each galaxy respectively obtained up to where the velocity field is ordered for each galaxy, the dispersion associated with the averaged value of pixels within the same sector is indicated with bars.

north side of *NGC* 6090 *NE* the gas approaches us, while in the south the gas moves away. Its maximum rotational velocity reaches $V_{\Theta \max} = 130 \pm 5 \text{ km s}^{-1}$ at 3 arcsec to the south from its kinematic center.

The rotation curve of *NGC* 6090 *SW* (bottom right panel of Figure 4) was obtained with pixels in the velocity field within an angular sector of 60° around the kinematic major axis of the galaxy. The physical coordinates of the kinematic centre are $\alpha_{J2000} = 16^h 11^m 40.42^s$, $\delta_{J2000} = +52^\circ 27' 22''.21$. The kinematic centre used to compute the rotation curve in this galaxy matches the photometric centre within 0.77 arcsec. The kinematic parameters that reduce significantly the asymmetry and scatter in the rotation curve inside of the radius $R = 4.5$ arcsec were, in this case, $PA = 26^\circ \pm 3$, $i = 64.8^\circ \pm 0.5$, and $V_{\text{sys}} = 8890 \text{ km s}^{-1}$. Just as we calculated the heliocentric distance for *NGC* 6090 *NE*, we have obtained that the heliocentric distance of *NGC* 6090 *SW* is 118 Mpc. The rotation curve of *NGC* 6090 *SW* shows that the north side is blue-shifted as well as the northeastern galaxy. The maximum rotational velocity of *NGC* 6090 *SW* is $V_{\Theta \max} = 132 \pm 5 \text{ km s}^{-1}$ at 2 arcsec to the north from its kinematic center.

In the rotation curve of *NGC* 6090 *SW* there is a point on the receding side with high dispersion associated to the average of the radial velocities computed using only two pixels of the velocity field, the pixel on the kinematic centre considered the framework to draw the radial velocities in the rotation curve and hence, considered the point with the lowest radial velocity value, and the pixel at the southwest of the kinematic center with the highest radial velocity value of the velocity field of all the system. Despite of that, we decided to use this point only to get a better view of the rotation curve of this galaxy toward the south.

4.3. Velocity dispersion field

Through the Full Width at Half Maximum (FWHM) of Gaussian functions fitted to the velocity profile of the H α line in each pixel, we obtained the velocity dispersion map of the galaxy system. Figure 5 displays the velocity dispersion map of *NGC* 6090 with the NICMOS/HST image overlaid. In *NGC* 6090 *NE* the velocity dispersion increase gradually from $\sim 45 - 55 \text{ km s}^{-1}$ in the eastern side of the galaxy, to $59 - 66 \text{ km s}^{-1}$ in the centre, and then up to 75 km s^{-1} in its north-western spiral arm near of what might look like a bridge between the galaxies. In *NGC* 6090 *SW*, the velocity dispersion maximum is 85 km s^{-1} next to the position of its photometric centre, then in its surroundings the velocity dispersion range is $\sim 40 \text{ km s}^{-1}$ increasing to the north, where it is $\sim 69 \text{ km s}^{-1}$.

In the north side of galaxy system and between both galaxies, broader profiles were noticed by double radial velocity profiles with low signal to noise ratio that we detected with PUMA mainly located in the bridge zone. Those broader profiles have been already detected by Cortijo-Ferrero et al. (2017) and interpreted as a consequence of shocks in early-stage mergers. This feature of the velocity dispersion field indicates that *NGC* 6090 has an interaction

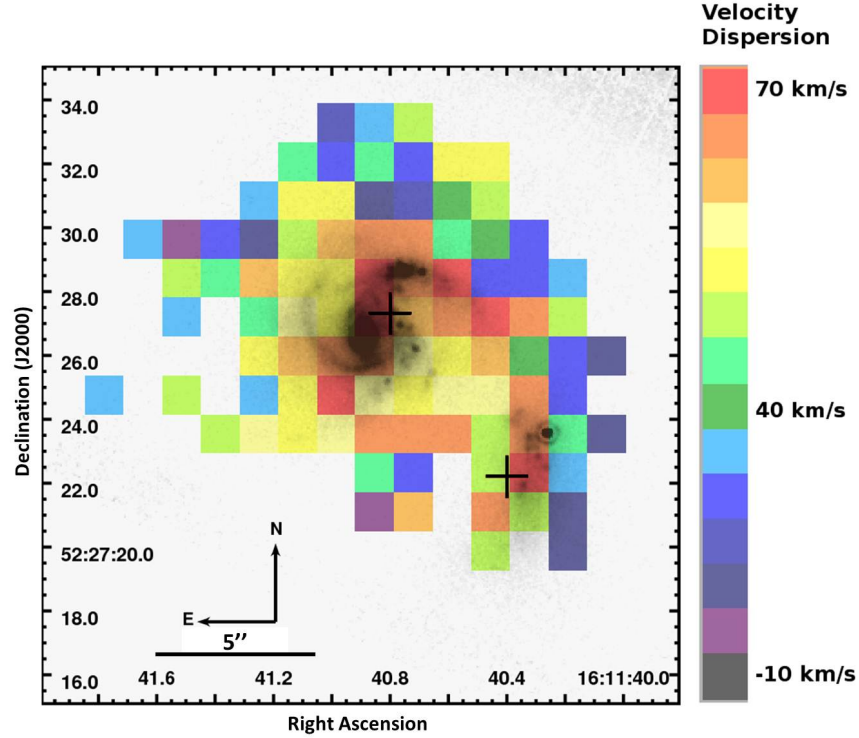


Fig. 5. Velocity dispersion map obtained using the PUMA in a 22 arcsec field of view centred on *NGC* 6090 superimposed on the NICMOS/HST 2.22 μm image. Symbols ‘+’ represent the photometric centre of each galaxy.

bridge between its galaxies. Those pixels with double velocity profiles are outside of the ordered velocity field of each galaxy, so that they do not contribute to any point in the computation of the rotation curves, moreover, given their low signal to noise ratio we do not consider them in this work.

4.4. The rotation sense of *NGC* 6090 NE

Radial-velocity measurements cannot by themselves distinguish leading and trailing spirals in thin disks. To determine whether a given galaxy leads or trails, we must determine which side of the galaxy is closer to us. Thus, to determine if the galaxies in *NGC* 6090 lead or trail, we followed the gradient criterion of Pasha (1985): the apparent brightness of the nuclear region falls off unequally from the centre outward along the minor axis, the far side being the one where the surface-brightness profile declines more smoothly. It means, if the inner disc is dusty, so it absorbs a significant fraction of the starlight passing through it, then the surface brightness of the bulge at a given distance along its apparent minor axis will be lower on the near side (Binney & Tremaine 1987). In this way, for each galaxy in the *NGC* 6090 was obtained

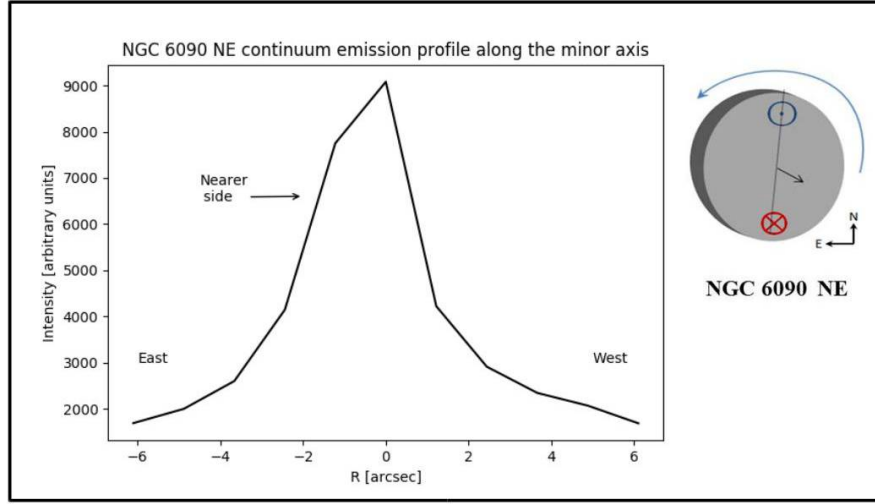


Fig. 6. Intensity profile of the continuum map of *NGC* 6090 *NE* along the minor axis centred on the galactic photometric center. Following the gradient criterion of Pasha (1985), the far side of the galaxy would be that one that falls more smoothly, therefore the nearest side to the observer of *NGC* 6090 is the eastern one. Top-right panel shows a scheme of 3D orientation of *NGC* 6090 *NE* derived from our kinematic analysis.

the intensity profile of the continuum emission of their minor axis in order to know the rotation sense of each one.

For *NGC* 6090 *NE*, we extracted the intensity profile of the continuum from its minor photometric axis (see Figure 2 in § 3), as it is shown in Figure 6. This profile indicates that the nearest side to the observer is the eastern side of the galaxy. Then, considering that the rotation curve indicates that the gas on the northern side is blue-shifted and helping us with the dust lanes which trace the arms structure of this galaxy (see right panel of Figure 1), we can infer that this galaxy has its arms rotating in a trailing direction.

On the other hand, for *NGC* 6090 *SW* it was not possible to obtain an accurate result through which we might determine its rotation sense due to the low number of pixels with continuum emission along its minor axis, but in addition, the image of $2.22\ \mu\text{m}$ do not mark clearly the structure of spiral arms.

5. MASS ESTIMATES USING DYNAMICAL ANALYSIS

A range of possible values for the mass of each galaxy in the *NGC* 6090 system was calculated using the approach described by Lequeux (1983), as has been done before when studying pairs of galaxies (e.g. Amram et al. 1992; Fuentes-Carrera et al. 2007; Repetto et al. 2010). This approach consists in calculating the mass $M(R)$ up to a certain radius where the rotation velocity $V(R)$ has been measured. The method considers two extreme cases to

evaluate the mass of galaxies: the galaxy seen as a flat disc and the galaxy described as a spherical system. Thus, the mass of the spiral galaxies is in the range of $M(R) = \kappa R V^2(R)/G$, where G is the gravitational constant and the coefficient κ is an element of the range (0.6, 1.0), whose limiting values correspond to the galaxy being dominated by a flat disc or by a massive spherical halo, respectively.

Thus, from the *NGC* 6090 *NE* rotation curve, the maximum rotation velocity of this galaxy is $V_{NE} = 130 \text{ km s}^{-1}$ which is reached at a radius of $R = 2.47 \text{ arcsec}$. For this galaxy the mass range obtained is $M_{NE} = \kappa 1.26 \times 10^{10} M_{\odot}$. From *NGC* 6090 *SW* rotation curve, the maximum rotation velocity is $V_{SW} = 132 \text{ km s}^{-1}$ reached at $R = 1.97 \text{ arcsec}$. For this galaxy the mass range is $M_{SW} = \kappa 1.05 \times 10^{10} M_{\odot}$. Therefore, the sum of both masses in the case of both galaxies being dominated by a massive spherical halo is $M_{sph} = 2.31 \times 10^{10} M_{\odot}$, and in the case of both galaxies being dominated by flat disc, the mass is $M_{flat} = 1.39 \times 10^{10} M_{\odot}$.

When two galaxies of roughly equal mass have an encounter, their extended halos may merge to form a common halo, then the galaxies are expected to orbit in a common halo until dynamical friction and tidal interactions have removed sufficient orbital energy for the galaxies to merge (e.g. Binney & Tremaine 1987; Mo et al. 2010). Thus, due to the high state of interaction of the galaxies forming part of *NGC* 6090 it is possible infer that they are dominated by a flat disc individually, but a further study on the dynamics of this encounter would be necessary to dismiss the probably case in which both galaxies are dominated by an spherical halo.

A second independent way of obtaining the mass value of a pair of galaxies is the method proposed by Karachentsev (1987), which calculates the mass of the pair from the relative orbital motion of the components of the pair. This method consists of assuming that the components of the pair move in a circular orbit with a velocity V_{12} and spatial separation r . When V_{12} and r are transformed into observable quantities, they become the difference of the velocity projected in the line of view, $y = V_{12} \sin i \cos \Omega$, and the separation projected on the sky plane, $X = r(1 - \sin^2 i \sin^2 \Omega)^{1/2}$, where i is the angle between the plane of the orbit and the plane of the sky, and Ω the angle between the line of view and the line connecting the both galaxies of the pair. For a circular motion, Karachentsev (1987) obtained the projection factor $\langle \eta \rangle = 3\pi/32$. Therefore, the total mass of the pair is:

$$M = \frac{32}{3\pi} \frac{X y^2}{G}, \quad (2)$$

where G is the gravitational constant. As y and X depend on a sinusoidal function, in order to obtain the upper limit of mass with this method and without loss of generality, for *NGC* 6090 we assumed that the orbital plane has an inclination of $i = 90^\circ$. Then, the angle between the line of sight and the line connecting the pair is $\Omega = \sin^{-1}(L/D)$, where $L = 4.1 \text{ kpc}$ is the distance of the nuclei projected on the sky plane and $D = 133.1 \text{ kpc}$ is the size of the line connecting the galaxies, which results in $\Omega = 1.76^\circ$. Thus, the

velocity projected on the line of view and the separation projected on the sky plane is $y \approx V_{12}$ and $X \approx r$. Assuming a circular orbit, the total mass would be:

$$M_{\text{orbital}} = \frac{32}{3\pi} \frac{r V_{12}^2}{G}, \quad (3)$$

where V_{12} is the difference between the system velocities of the galaxies, r is the projected separation between the nucleus of each galaxy. For the galaxy system *NGC* 6090 we have, $V_{12} = 10 \text{ km s}^{-1}$ and $r = 4.1 \text{ kpc}$. Therefore, the orbital mass is $M_{\text{orbital}} = 3.23 \times 10^8 M_{\odot}$, which is two orders of magnitude lower than the sum of individual masses obtained with the method proposed by Lequeux (1983). We think that this low value of the mass is due to the fact that the projected velocity difference V_{12} is quite small.

6. DISCUSSION

At optical wavelengths, *NGC* 6090 appears as a double nuclei system with two curved antennas (tidal tails), so that this galaxy system has been described similar to *NGC* 4038/39 (The Antennae) (e.g. Toomre & Toomre 1972; Martin et al. 1991; Mazzarella & Boroson 1993; Dinshaw et al. 1999; Bryant & Scoville 1999). With the goal of studying kinematic similarities between both pairs of galaxies produced by the interaction of their own galaxies, we studied the H α kinematics of *NGC* 6090 using the scanning Fabry-Perot interferometer, PUMA. The H α kinematics of the galaxy pair The Antennae has been studied through observations obtained with another FP by Amram et al. (1992). In both galaxy systems, *NGC* 6090 and The Antennae, no emission of ionized hydrogen was detected in their tidal tails, i.e. in both galaxy systems, ionized gas emitting at H α was only detected in the central zone, respectively. Therefore, Amram et al. (1992) performed a kinematic analysis of the disc of The Antennae, as well as we have done for *NGC* 6090 in this paper.

Amram et al. (1992) reported that in The Antennae, ionized gas emitting at H α is deficient compared with its continuum emission, but these emissions tend to grow into its farthest part to its companion. Then, the The Antennae nuclei matched unambiguously with observations at $2.2 \mu\text{m}$. The velocity field is not ordered throughout the system, none of its component galaxies show the behavior of a rotating disc. Additionally, there were not detected pixels with double velocity profiles. Finally, using the Lequeux (1983) method to measure the mass of the galaxies, Amram et al. (1992) found that the individual mass of the galaxies in The Antennae is approximately $2 \times 10^{10} M_{\odot}$ for each one.

For *NGC* 6090, in § 3, we observed that the intensity of ionized gas emitting at H α is lower with respect to that of the continuum, but within each galaxy, the ionized hydrogen gas approaches to its companion, while the old stellar population is lagging in the opposite direction. The positions of the nuclei reported at $2.22 \mu\text{m}$ by Dinshaw et al. (1999), the HI continuum maxima reported by Condon et al. (1990) and the monochromatic and continuum H α maxima that we obtained in this paper on the NICMOS/HST image, are indicated in Figure 7.

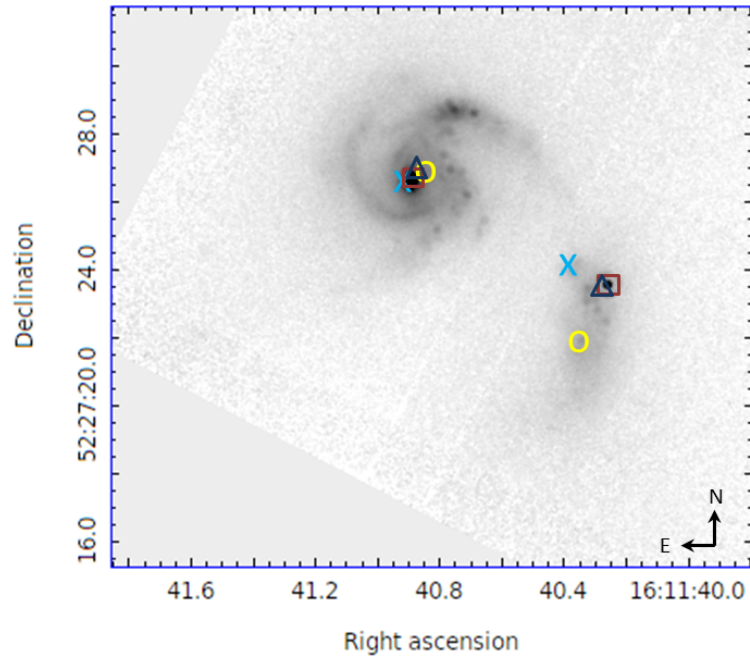


Fig. 7. NICMOS/HST image at $2.22 \mu\text{m}$ of a field of view of 16 arcsec centered at *NGC* 6090. In this image we have marked the positions of the maximum emissions of the continuum (O), the $\text{H}\alpha$ monochromatic emission (Δ), the radio continuum (X) and the infrared (\square).

For *NGC* 6090 *NE*, we observed that the maxima of the monochromatic and continuum of the observation made with PUMA almost completely coincide and match with the kinematic centre within 0.4 arcsec. In Figure 7 we observe that the differences between the position of the nucleus of this galaxy reported in the literature so far and our results are minimal.

However, for the galaxy *NGC* 6090 *SW* the maxima of the continuum and the monochromatic emissions derived from our observations of the ionized gas emitting at H α show that they are not almost in the same position as those in *NGC* 6090 *NE*. This galaxy presents greater emissions of ionized hydrogen towards the north than to the south, so that the photometric maximum is located to the south while the maximum monochromatic emission is in the north. Thus, for *NGC* 6090 *SW*, the position of the monochromatic emission maximum is $\alpha_{J2000_{H\alpha}} = 16^h 11^m 40.3^s$, $\delta_{J2000_{H\alpha}} = +52^\circ 27' 23''$, and the maximum of the continuum is $\alpha_{J2000_{cont}} = 16^h 11^m 40.4^s$, $\delta_{J2000_{cont}} = +52^\circ 27' 22''$ which match with the kinematic centre and the velocity dispersion maximum. The maximum of the 2.22 μm emission is in $\alpha_{J2000} = 16^h 11^m 40.3^s$, $\delta_{J2000} = +52^\circ 27' 23''$ (Dinshaw et al. 1999), and the maximum radio continuum is in $\alpha_{J2000} = 16^h 11^m 40.8^s$, $\delta_{J2000} = +52^\circ 27' 27''$ (Hummel et al. 1987; Condon et al. 1990).

Dinshaw et al. (1999) compared the position of the brightest point in the 2.22 μm image with the maximum of the radio-continuum of this galaxy, proposing that the infrared peak could be a field star. However, the emission of a field star could not be detected as the maximum of the redshifted H α line of our observations of *NGC* 6090, therefore, it may be concluded that the infrared maximum for the southwestern galaxy is a component itself. This possibility is supported by Cortijo-Ferrero et al. (2017), who argued that the main absorption lines of their observations in the range from 3700 to 7100 Å at the knot of 2.22 μm have the same redshift of the galaxy. But also, Cortijo-Ferrero et al. (2017) obtained that the position of the continuum maximum is southward of the infrared peak, near from where we detected the continuum maximum, the kinematic centre and the velocity dispersion maximum of *NGC* 6090 *SW*. Thus, taking the maximum of the H α continuum as the nucleus of the southwest galaxy, we determined that the separation of the nuclei of the two members of *NGC* 6090 is 7.11 arcsec. Assuming that the average distance of the galaxy system *NGC* 6090 is 118 Mpc, the distance between its nuclei is 4.1 kpc.

Regarding the velocity field of *NGC* 6090, we said in § 4.1 that this galaxy system has two ordered velocity fields which allowed us to compute the rotation curves of each galaxy in the *NGC* 6090 system. The rotation curves have higher maxima rotational velocity values than the dispersion or residual velocity fields: the northeast galaxy has maximum rotational velocity $V_{NE} = 130 \text{ km s}^{-1}$ and its velocity dispersion is in the range $\sim 45 - 66 \text{ km s}^{-1}$ inside of its disc; meanwhile *NGC* 6090 *SW* has maximum rotational velocity $V_{SW} = 132 \text{ km s}^{-1}$, with its velocity dispersion in the range $\sim 40 - 69 \text{ km s}^{-1}$ inside the disc. Both galaxies reached their maximum velocity dispersion out-

side the disc but even these values were still less than their maxima rotational velocities.

Besides, with the continuum map obtained from our observations, the asymmetric isovelocities contour curves and the non-circular motions that we detected in *NGC 6090 NE*, we confirmed the assumption about the presence of a bar structure in this galaxy made in the infrared by Dinshaw et al. (1999) (see figure 2 of their paper) and at optical wavelengths by Cortijo-Ferrero et al. (2017).

In their paper, Amram et al. (1992) concluded that the encounter of the galaxies that make up The Antennae are in an advanced stage of interaction. In the case of *NGC 6090*, the features that we have discussed above about its two ordered velocity fields, continuum and monochromatic maps, and the behaviour of its velocity dispersion field that signals an interaction bridge between galaxies, allow us to conclude that *NGC 6090* is a system in a less advanced stage of interaction than The Antennae, although both systems are in an interaction stage previous to a merger.

Regarding the mass values, Table 4 contains the values of the masses reported in the literature for the *NGC 6090* system at different wavelengths compared to our results. The range of the sum of independent masses estimated in this paper with the rotation curves of each galaxy in the *NGC 6090* system obtained with the method by Lequeux (1983) has the same order of magnitude as the masses estimated by other authors in the infrared (Sanders et al. 1991; Bryant & Scoville 1999; Chisholm et al. 2016a; Cortijo-Ferrero et al. 2017) and radio continuum (Martin et al. 1991), which were determined by means of the mass-to-light ratio. However, the mass of the *NGC 6090* system calculated with the method proposed by Karachentsev (1987) is two orders of magnitude smaller than those values, and it has an order of magnitude less as the dynamic mass estimated by Bryant & Scoville (1999).

The sum of masses computed with the maximum rotation velocity coincide in order of magnitude with the masses acquired from the mass-to-light ratio at other wavelengths, even, they have the same value determined by Sanders et al. (1991) and Bryant & Scoville (1999), either if each galaxy is dominated by a flat disc or an spherical halo, which allow us to argue that the kinematic parameters that we obtained in this work are reliable. Thus, the difference of one order of magnitude with the orbital mass can be consequence to our geometrical assumptions of the movement of *NGC 6090 SW* around of its companion.

Most of the numerical simulations have taken similar initial conditions to model different features of The Antennae (e.g. Toomre & Toomre 1972; Barnes 1988; Teyssier et al. 2010; Renaud et al. 2008, 2015), either its morphology or the formation of star clusters during the merger, obtaining all the times the same feature of two long tidal tails that form the antennae. Therefore, in general, the symmetry of the tidal action allows the formation of four arms if the two companions are disc galaxies, when the masses of the two interacting galaxies are equal or of the same order, the two internal spiral arms join up

TABLE 4
 MASSES OF THE GALAXY SYSTEM *NGC* 6090 FOUND IN
 DIFFERENT WAVELENGTHS IN THE LITERATURE COMPARED
 WITH THE ONES THAT WE FOUND IN THIS WORK.

Author	Phase of the IM observed	Mass [$M_{\odot} \times 10^{10}$]
Sanders et al. (1991)	H ₂	1.4
Bryant & Scoville (1999)	H ₂ (dyn)	0.46
	H ₂ (gas)	2.29
Hummel et al. (1987)	HI	3.9
Chisholm et al. (2016a)	MIR	5.02
Cortijo-Ferrero et al. (2017)	MIR	4.2
Cortijo-Ferrero et al. (2017)	3650 – 6950 Å	6.8
This work	H α _{sum flat disc}	1.39
	H α _{sum sph halo}	2.31
	H α _{orbital}	0.032

to form a bridge, the two external arms are drawn into two *antennae* which remain for one or two billion years (Combes et al. 2002). This phenomenon is happening with the galaxies of *NGC* 6090, which have similar mass values, we note the two tidal tails and the bridge between them well defined by the northwestern arm of *NGC* 6090 *NE*.

Finally, Sugai et al. (2004) observed young starbursts occurring in regions offset from the galactic nuclei to the northwestern spiral arm of *NGC* 6090 *NE*. They inferred that if *NGC* 6090 *NE* had its arms trailing, the molecular gas clouds in that arm were just finishing an interaction with the central molecular gas. In § 4.4 we showed that the spiral arms in the north-eastern galaxy are trailing enforcing this theory. Another likely consequence of the trailing arms of *NGC* 6090 *NE* could be the outflow in the northeastern side of *NGC* 6090 *SW* detected by Chisholm et al. (2016b) in the UV band (see figure 1 of their paper) that coincides with a region with H α high velocity dispersion zone on *NGC* 6090 *SW*, which apparently could have been formed by ram pressure during the interaction.

7. CONCLUSIONS

In this paper we present our observations of the ionized gas emitting at H α of the isolated pair of galaxies *NGC* 6090 (*KPG* 486) carried out with the scanning Fabry-Perot interferometer, PUMA. This emission was detected solely in the central area of the system. Through our observations we obtained the monochromatic emission (ionized gas emitting at H α), the continuum, the velocity field and the velocity dispersion maps. The velocity field of *NGC* 6090

shows two regions with ordered isovelocities contour curves from which we computed the rotation curve of each galaxy of the pair.

Using the rotation curves, we obtained the maximum rotation velocity, the mass of each galaxy, and the mass of the galaxy system. The sum of the individual masses that we calculated is consistent with the masses found in the literature, obtained with the mass-to-light ratio for different wavelengths. In addition, we obtained the orbital mass of *NGC* 6090, which differs in two orders of magnitude in relation to the sum of the individual masses. We conclude that this difference is due to projection effects.

In addition, enough emission was detected in the northeast galaxy to observe the specific characteristics therein. In this galaxy, the isophotes of the continuum show signs of a stellar bar, the velocity field shows no symmetry with respect to the minor axis, which in turn suggest that this galaxy does have a stellar bar. And, it was also possible to conclude that the arms of *NGC* 6090 *NE* galaxy rotate in a trailing direction.

We concluded that the photometric centre of the southwest galaxy is in a different location than those reported from radio and infrared wavelengths, which were inconsistent. Furthermore, the maximum of ionized gas emitting at $H\alpha$ and the maximum of the $2.22\ \mu\text{m}$ coincide, confirming that this knot is part of the galaxy, and therefore it cannot be a field star. However, we were not able to study the morphological characteristics of the southwestern galaxy due to the size of the emission area that was detected.

As regards optical wavelength images of *NGC* 6090, the system is similar to The Antennae (*NGC* 4038/39), while also it has been defined as a merger. In this paper we have discussed the kinematic differences between these galaxy systems with observations made at the same wavelength with similar instruments, which allowed us to conclude that their differences are mainly due to the stage of interaction of the galaxies that make up these systems. Through the kinematic analysis of *NGC* 6090 we concluded that their galaxies are in a previous stage of merger than those galaxies in The Antennae.

Acknowledgements

Our research was carried out thanks to the Program UNAM-DGAPA-PAPIIT IN109919.

The authors express their gratitude to the Mexican National Council for Science and Technology (CONACYT) for financing this paper through the project CY-109919.

This paper is based on our observations performed with the scanning Fabry-Perot interferometer, PUMA, at the Observatorio Astronómico Nacional on Sierra San Pedro Mártir (OAN-SPM), Baja California, México.

We thank the daytime and night support staff at OAN-SPM for facilitating and helping to obtain our observations.

The Digitized Sky Surveys were produced at the Space Telescope Science Institute under U.S. Government grant NAG W-2166. The images of these surveys are based on photographic data obtained using the Oschin Schmidt

Telescope on Palomar Mountain and the UK Schmidt Telescope. The plates were processed into the present compressed digital form with the permission of these institutions.

REFERENCES

- Acosta-Pulido, J. A., Klaas, U., Laureijs, R. J., Schulz, B., Kinkel, U., Abraham, P., Castaneda, H. O., Cornwall, L., Gabriel, C., Heinrichsen, I., Herbstmeier, U., Krueger, H., & Pelz, G. 1996, *A&A*, 315, L121
- Amram, P., Marcelin, M., Boulesteix, J., & Le Coarer, E. 1992, *A&A*, 266, 106
- Amram, P., Plana, H., Mendes de Oliveira, C., Balkowski, C., & Boulesteix, J. 2003, *A&A*, 402, 865
- Arp, H. 1966, *ApJS*, 14, 1
- Barnes, J. E. 1988, *ApJ*, 331, 699
- Barnes, J. E. & Hernquist, L. 1992, *ARA&A*, 30, 705
- Binney, J. & Tremaine, S. 1987, *Galactic dynamics*
- Bosma, A. 1981, *AJ*, 86, 1825
- Bryant, P. M. & Scoville, N. Z. 1999, *AJ*, 117, 2632
- Cárdenas-Martínez, N. & Fuentes-Carrera, I. 2018, *ApJ*, 868, 141
- Chamberlain, J. W. 1961, *Physics of the aurora and airglow*
- Chisholm, J., Tremonti, C. A., Leitherer, C., Chen, Y., & Wofford, A. 2016a, *MNRAS*, 457, 3133
- Chisholm, J., Tremonti, C. A., Leitherer, C., Chen, Y., Wofford, A., & Lundgren, B. 2015, *ApJ*, 811, 149
- Chisholm, J., Tremonti, A., Leitherer, C., & Chen, Y. 2016b, *MNRAS*, 463, 541
- Combes, F., Boisse, P., Mazure, A., Blanchard, A., & Seymour, M. 2002, *Galaxies and cosmology*
- Condon, J. J., Helou, G., Sanders, D. B., & Soifer, B. T. 1990, *ApJS*, 73, 359
- Cortijo-Ferrero, C., González Delgado, R. M., Pérez, E., Cid Fernandes, R., Sánchez, S. F., de Amorim, A. L., Di Matteo, P., García-Benito, R., Lacerda, E. A. D., López Fernández, R., & Tadhunter, C. 2017, *MNRAS*, 467, 3898
- Dinshaw, N., Evans, A. S., Epps, H., Scoville, N. Z., & Rieke, M. 1999, *ApJ*, 525, 702
- Epinat, B., Amram, P., Marcelin, M., Balkowski, C., Daigle, O., Hernandez, O., Chemin, L., Carignan, C., Gach, J.-L., & Balard, P. 2008, *MNRAS*, 388, 500
- Fuentes-Carrera, I., Cárdenas-Martínez, N., Sánchez-Cruces, M., Rosado, M., Amram, P., Olguín, L., Borissova, J., Verley, S., Flores, H., Verdes-Montenegro, L., & Gonçalves, D. 2015, 309, 314
- Fuentes-Carrera, I., Rosado, M., Amram, P., Dultzin-Hacyan, D., Cruz-González, I., Salo, H., Laurikainen, E., Bernal, A., Ambrocio-Cruz, P., & Le Coarer, E. 2004, *A&A*, 415, 451
- Fuentes-Carrera, I., Rosado, M., Amram, P., Salo, H., & Laurikainen, E. 2007, *A&A*, 466, 847
- Gabbasov, R. F., Rosado, M., & Klapp, J. 2014, *ApJ*, 787, 39
- Günthardt, G. I., Díaz, R. J., & Agüero, M. P. 2016, *AJ*, 152, 150
- Hubble, E. 1936, *ApJ*, 84, 517
- Hummel, E., van der Hulst, J. M., Keel, W. C., & Kennicutt, Jr., R. C. 1987, *A&AS*, 70, 517

- Karachentsev, I. 1987, Double galaxies
- Krassovsky, V. I., Shefov, N. N., & Yarin, V. I. 1962, Atlas of the airglow spectrum 3000-12400 Å
- Lequeux, J. 1983, *A&A*, 125, 394
- Makarov, D., Prugniel, P., Terekhova, N., Courtois, H., & Vauglin, I. 2014, *A&A*, 570, A13
- Martin, C. L. & Soto, K. T. 2016, *ApJ*, 819, 49
- Martin, J. M., Bottinelli, L., Gouguenheim, L., & Dennefeld, M. 1991, *A&A*, 245, 393
- Mazzarella, J. M. & Boroson, T. A. 1993, *ApJS*, 85, 27
- Mihalas, D. & Binney, J. 1981, *Galactic astronomy: Structure and kinematics*, 2nd edn.
- Mihos, C. 2000, *Galaxies: Interactions and Mergers*, ed. P. Murdin, 2623
- Miralles-Caballero, D., Colina, L., Arribas, S., & Duc, P.-A. 2011, *AJ*, 142, 79
- Mo, H., van den Bosch, F. C., & White, S. 2010, *Galaxy Formation and Evolution NASA/IPAC*. 2014, *NASA/IPAC Extragalactic Database (NED)*, <https://ned.ipac.caltech.edu/>
- Noguchi, M. 1987, *MNRAS*, 228, 635
- Pasha, I. I. 1985, *Soviet Astronomy Letters*, 11, 1
- Renaud, F., Boily, C. M., Fleck, J.-J., Naab, T., & Theis, C. 2008, *MNRAS*, 391, L98
- Renaud, F., Bournaud, F., & Duc, P.-A. 2015, *MNRAS*, 446, 2038
- Repetto, P., Rosado, M., Gabbasov, R., & Fuentes-Carrera, I. 2010, *AJ*, 139, 1600
- Rosado, M., Gabbasov, R., & Fuentes-Carrera, I. 2011, 277, 259
- Rosado, M., Gabbasov, R. F., Repetto, P., Fuentes-Carrera, I., Amram, P., Martos, M., & Hernandez, O. 2013, *AJ*, 145, 135
- Rosado, M., Langarica, R., Bernal, A., Cobos, F., Garfias, F., Gutierrez, L., Tejada, C., Tinoco, S., & Le Coarer, E. 1995, 3, 263
- Salo, H. & Laurikainen, E. 2000a, *MNRAS*, 319, 377
- . 2000b, *MNRAS*, 319, 393
- Sanders, D. B., Scoville, N. Z., & Soifer, B. T. 1991, *ApJ*, 370, 158
- Schweizer, F. 1986, *Science*, 231, 227
- Sugai, H., Davies, R. I., Ishii, M., & Ward, M. J. 2000, *MNRAS*, 317, 447
- Sugai, H., Hattori, T., Kawai, A., Ozaki, S., Kosugi, G., Ohtani, H., Hayashi, T., Ishigaki, T., Ishii, M., Sasaki, M., & Takeyama, N. 2004, *ApJ*, 615, L89
- Teyssier, R., Chapon, D., & Bournaud, F. 2010, *ApJ*, 720, L149
- Toomre, A. & Toomre, J. 1972, *ApJ*, 178, 623
- Torres-Flores, S., Amram, P., Mendes de Oliveira, C., Plana, H., Balkowski, C., Marcelin, M., & Olave-Rojas, D. 2014, *MNRAS*, 442, 2188
- Vollmer, B., Marcelin, M., Amram, P., Balkowski, C., Cayatte, V., & Garrido, O. 2000, *A&A*, 364, 532
- Vorontsov-Velyaminov, B. A., Noskova, R. I., & Arkhipova, V. P. 2001, *Astronomical and Astrophysical Transactions*, 20, 717
- Wang, J., Zhang, Q., Wang, Z., Ho, P. T. P., Fazio, G. G., & Wu, Y. 2004, *ApJ*, 616, L67

Margarita Rosado: Instituto de Astronomía, Universidad Nacional Autónoma de México (UNAM). Apdo. Postal 70-264, 04510, Ciudad de México, México (margarit@astro.unam.mx).

Minerva Muñoz Sardaneta and Mónica Sánchez-Cruces: Aix Marseille Univ, CNRS, CNES, Laboratoire d'Astrophysique de Marseille (LAM). 38 rue F. Joliot-Curie, 13388 Marseille cedex 13 France (minerva.munoz@lam.fr).